SAND2018-10598R

Built on LDRD Laboratory Directed Research and Development

SAND2018-XXXXR
LDRD PROJECT NUMBER: 211659
LDRD PROJECT TITLE: Three-Dimensional Imaging through Shock-Waves at Ultra-High Speed
PROJECT TEAM MEMBERS: Yi Chen Mazumdar, Michael E. Smyser, Jeffery D. Heyborne, and Daniel R. Guildenbecher

ABSTRACT:

Imaging diagnostics that utilize coherent light, such as digital in-line holography, are important for object sizing and tracking applications. However, in explosive, supersonic, or hypersonic environments, gas-phase shocks impart imaging distortions that obscure internal objects. To circumvent this problem, some research groups have conducted experiments in vacuum, which inherently alters the physical behavior. Other groups have utilized single-shot flash x-ray or high-speed synchrotron x-ray sources to image through shock-waves. In this work, we combine digital in-line holography with a phase conjugate mirror to reduce the phase distortions caused by shock-waves. The technique operates by first passing coherent light through the shock-wave phase-distortion and then a phase-conjugate mirror. The phase-conjugate mirror is generated by a four-wave mixing process to produce a return beam that has the exact opposite phase-delay as the forward beam. Therefore, by passing the return beam back through the phase-distortion, the phase delays picked up during the initial pass are canceled, thereby producing improved coherent imaging. In this work, we implement phase conjugate digital in-line holography (PCDIH) for the first time with a nanosecond pulse-burst laser and ultra-high-speed cameras. This technique enables accurate measurement of the three-dimensional position and velocity of objects through shock-wave distortions at video rates up to 5 MHz. This technology is applied to improve three-dimensional imaging in a variety of environments from imaging supersonic shock-waves through turbulence, sizing objects through laser-spark plasma-generated shock-waves, and tracking explosively generated hypersonic fragments. Theoretical foundations and additional capabilities of this technique are also discussed.

1 INTRODUCTION:

Many environments from hypersonics to explosives, create imaging challenges plagued by optical distortions due to shock-waves. Current state-of-the-art experiments conducted by Los Alamos and Argonne use synchrotron x-rays [1] to overcome shock-waves while capturing a maximum of four images per experiment at 6.7 million frames-per-second [2]. To construct three-dimensional pictures, multiple repetitions with different views are required [2]. Ultimately, diagnostics that

Sandia National Laboratories is a multimission laboratory managed and operated by National Technology and Engineering Solutions of Sandia, LLC, a wholly owned subsidiary of Honeywell International, Inc., for the U.S. Department of Energy's National Nuclear Security Administration under contract DE-NA-0003525.

Sandia National Laboratories

U.S. DEPARTMENT OF ENERGY

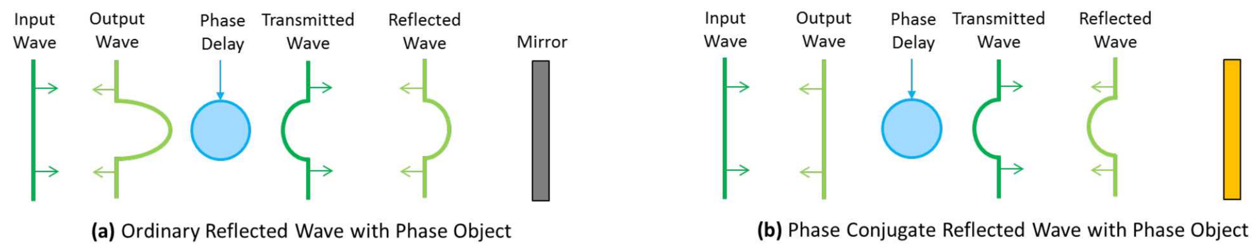

Figure 1: *Distortions produced by phase objects, such as a shock-wave, are illustrated for (a) an normal mirror and (b) a phase conjugate mirror.*

operate outside of synchrotron facilities and capture 3D transient information from a single experiment are needed.

Digital in-line holography (DIH) is a single-shot method used for accurately tracking the three-dimensional (3D) motion of high speed objects in flow [3, 4, 5, 6] and combustion [7, 8, 9, 10, 11] environments. In addition to the ability to freeze motion, DIH only requires optical access along a single line of sight to produce 3D position estimates [12, 13]. Since DIH uses coherent interference of laser light, however, it is susceptible to phase disturbances in the imaging beam path. For explosive environments [14], shock-waves created by gas-phase density gradients can cause severe distortions in holograms, making implementation of DIH impractical in these situations. In addition, ultra-high-speed laser and camera systems are required to obtain video-rate images for these and other ultra-high-speed applications.

Several new laser systems currently exist that could potentially be used for diagnostics in explosive environments. Pulse-burst lasers have been recently applied to transonic wind tunnels for particle image velocimetry [15], turbulent flame environments for laser induced incandescence [16, 17], and time-resolved temperature measurements using coherent anti-Stokes Raman scattering spectroscopy [18] at rates of tens to hundreds of kilohertz (kHz). High power [19] and megahertz (MHz) rate [20] pulse-burst laser systems have also been constructed. New ultra-high-speed camera technologies from Kirana and Shimadzu [21] have also demonstrated frame rates up to 10 MHz. With these recent camera and laser developments, the last component required for creating video-rate holograms in explosive environments is a phase distortion canceling technique.

One possible method for eliminating phase distortions is to use a phase conjugate mirror [22] as illustrated in Fig. 1. The phase disturbance picked up by the imaging beam on its first pass through the phase object can be sent into a phase conjugate mirror, which produces a backward propagating beam with a phase that is equal and opposite to the incoming beam. This beam can then be passed back through the object, effectively canceling the phase distortion while maintaining the ability to capture holograms from absorptive objects. Phase conjugate techniques have been previously applied to remove imaging distortions [23, 24, 25, 26] and since phase conjugation is a nonlinear technique, it also has applications in removing amplified spontaneous emission [27] and modal dispersion [28]. Phase conjugation has also previously been applied to create holograms using

Sandia National Laboratories is a multimission laboratory managed and operated by National Technology and Engineering Solutions of Sandia, LLC, a wholly owned subsidiary of Honeywell International, Inc., for the U.S. Department of Energy's National Nuclear Security Administration under contract DE-NA-0003525.

film [29] and using spatial light modulators [30, 31, 32]. Unfortunately, these particular holographic techniques are incompatible with the ultra-high-speed imaging requirements of explosive environments. Thus alternative optical techniques are required.

In order to meet the ultra-high-speed imaging requirements of explosive environments, we have combined DIH with a phase conjugate mirror for single-shot optical phase distortion cancellation with picosecond [33] and nanosecond [34] lasers. In this report, we further incorporate MHz-rate cameras and MHz-rate pulse-burst lasers to create an ultra-high-speed phase conjugate digital in-line holography (PCDIH) technique for capturing MHz 3D videos of explosive fragments. Due to laser power limitations, previous work has only been implemented at 10 to 20 Hz repetition rates [33, 34]. Operating up to 5 MHz would show more than five orders-of-magnitude increase in speed. This work is the first to outline a MHz-rate PCDIH instrument capable of producing quantitative video-rate holograms in explosive, supersonic, and hypersonic environments.

We first begin by describing the theoretical foundations of DIH and PCDIH. Then, the experimental setup and implementation details for simultaneous DIH and PCDIH imaging is described for picosecond and nansecond laser systems. Results illustrating the ability to cancel distortions from stationary supersonic shock-waves, laser-spark plasma-generated shock-waves, and explosively-generated hypersonic fragments are then discussed. PCDIH images obtained from a pulse-burst laser and Shimadzu cameras are illustrated from 500 kHz up to 5 MHz. Additional features of the PCDIH configuration for shock-wave edge enhancement are also discussed.

2 PHASE CONJUGATE HOLOGRAPHY:

2.1 PHASE-CONJUGATE MIRROR:

Normal reflection with a conventional mirror can be compared with the phase-conjugate mirror in Fig. 1 by assuming an input wave of the form,

$$E(x,y,z,\omega) = A_0(x,y,z)e^{ikz-i\omega t}. \tag{1}$$

When this input wave passes through the phase disturbance, such as a density gradient, the transmitted wave picks up a phase delay ϕ such that,

$$E'(x,y,z,\omega) = A_0(x,y,z)e^{ikz+i\phi(x,y,z)-i\omega t}. \tag{2}$$

With the conventional mirror, the reflected wave and output wave after passing through the phase delay a second time are,

$$E''(x,y,z,\omega) = R_m A_0(x,y,z)e^{-ikz+i\phi(x,y,z)-i\omega t} \tag{3}$$

$$E'''(x,y,z,\omega) = R_m A_0(x,y,z)e^{-ikz+2i\phi(x,y,z)-i\omega t}. \tag{4}$$

This illustrates that the phase aberration is doubled. If a phase-conjugate mirror is used, the reflected and output waves are then,

$$E''(x,y,z,\omega) = R_{pc}A_0(x,y,z)e^{-ikz-i\phi(x,y,z)-i\omega t} \tag{5}$$

$$E'''(x,y,z,\omega) = R_{pc}A_0(x,y,z)e^{-ikz-i\phi(x,y,z)+i\phi(x,y,z)-i\omega t} = R_{pc}A_0(x,y,z)e^{-ikz-i\omega t}. \tag{6}$$

Thus, the output wave with a phase conjugate mirror cancels the distortions generated by the phase delay. A phase-conjugate mirror can be generated in several different ways. For this work, phase-conjugation is created via a degenerate four-wave-mixing process. This phase conjugate beam then interacts with objects to create interference patterns that can be numerically refocused to determine the depth at which objects are located in an image, which then enables three-dimensional object tracking.

2.2 DEGENERATE FOUR-WAVE MIXING:

Backward degenerate four-wave mixing phase-conjugation signal [22, 35] is generated when a third-order nonlinear medium is illuminated by two planar counter-propagating pump beams and a separate imaging beam that may contain some phase-delay wavefront distortion. This process is illustrated in Fig. 2. Note that a shallower angle between the pump beams and the imaging beam tends to increase the interaction length and generates wider interference fringes inside the medium [22], hence improving phase-conjugate signal. The three incident beams with frequency ω have electric fields of,

$$\mathbf{E_1}(\omega) = A_1(\mathbf{r})e^{-i(\omega t-\mathbf{k_1}\cdot\mathbf{r})} \tag{7}$$

$$\mathbf{E_2}(\omega) = A_2(\mathbf{r})e^{-i(\omega t-\mathbf{k_2}\cdot\mathbf{r})} \tag{8}$$

$$\mathbf{E_3}(\omega) = A_3(z)e^{-i(\omega t-\mathbf{k_3}\cdot z)}, \tag{9}$$

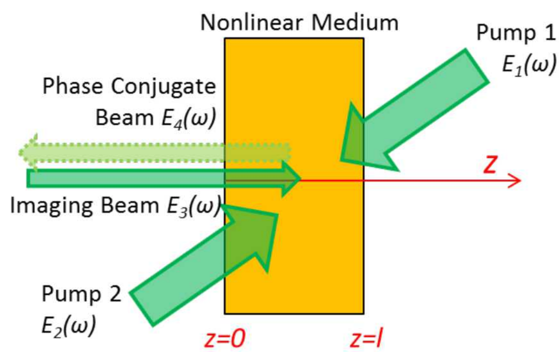

Figure 2: *A schematic of the degenerate four-wave-mixing process is illustrated.*

where $\mathbf{E}$ is the electric field, A is the real amplitude, and $\mathbf{k}$ is the wave vector. In this case, $\mathbf{k_1} = -\mathbf{k_2}$ due ot the counter-propagating configuration.

When these beams arrive at the medium simultaneously, a fourth beam with frequency ω is generated. From phase matching, we have $\mathbf{k_1} + \mathbf{k_2} = \mathbf{k_3} + \mathbf{k_4}$ resulting in the relation $\mathbf{k_3} = -\mathbf{k_4}$. The phase-conjugate beam propagates in the opposite direction as the original imaging beam due to these phase matching conditions. The resulting fourth beam has a third-order nonlinear electric polarization of,

$$\mathbf{P_4^{(3)}}(\omega) = \varepsilon_0 \chi_e^{(3)} A_1 A_2 A_3^* e^{-i(\omega t + \mathbf{k_3} \cdot z)}, \tag{10}$$

where $\chi_e^{(3)} = \chi^{(3)}(\omega, \omega, -\omega)$ is the effective third-order nonlinear susceptibility value. The equations describing the amplitude variation along the z-axis can be approximated as,

$$\frac{dA_3^*(z)}{dz} = i\gamma^* A_4(z) \tag{11}$$

$$\frac{dA_4(z)}{dz} = i\gamma A_4^*(z) \tag{12}$$

$$\gamma = \frac{\omega}{2cn_0(\omega)} \chi_e^{(3)} A_1 A_2. \tag{13}$$

Assuming that the pump beam amplitudes stay constant, the magnitude of the phase-conjugate signal is evaluated at one end of the media is,

$$A_4(0) = -i\frac{\gamma}{|\gamma|} \tan(|\gamma| l) A_3^*(0). \tag{14}$$

The resulting electric field of the phase-conjugate wave assuming small signal gains is then,

$$\mathbf{E_4}(\omega) = A_4(0) e^{-i(\omega t + \mathbf{k_3} \cdot z)}. \tag{15}$$

Notice that A_4 is proportional to A_3^*, which is the phase conjugate of the imaging beam A_3. The resulting reflectivity of the phase conjugate mirror can be calculated as,

$$R_{pc} = |A_4(0)|^2 / |A_3(0)|^2 = tan^2(|\gamma| l). \tag{16}$$

One additional consideration is the polarization of the three beams. Although many different configurations can be utilized, the p-, p-, and s-polarizations for the imaging, pump 1, and pump 2 beams respectively produces a phase-conjugate beam with an s-polarization. Since the imaging beam and phase-conjugate beam are polarized in different orientations, this enables more efficient separation of the two beams during imaging.

2.3 DIGITAL IN-LINE HOLOGRAPHY:

Digital holograms are produced from the coherent interference of light that is scattered by objects (object beam) with light that remains un-scattered (reference beam). For the in-line configuration, the object and reference both come from the same beam, producing two-dimensional (x and y) interference patterns that are collected at the holography image plane and can be numerically refocused along the optical depth z using the diffraction-integral equation,

$$E(x,y,z) = [h(x,y)E_r^*(x,y)] \otimes g(x,y,z). \tag{17}$$

Here, E is the reconstructed complex amplitude, h is the recorded hologram, E_r^* is the planar conjugate reference wave, $\otimes$ is the convolution operator, and g is the diffraction kernel. The refocused image at any depth z can be visualized using the amplitude $A = |E|$. The location of each amplitude object in the z-direction can be determined using a focus metric that aims to minimize amplitude and maximize edge sharpness. Additional refinement steps are then used to improve the z estimates and remove falsely detected or overlapped particles [36, 37, 12]. Once all the frames are processed, custom tracking software programs are used. These algorithms utilize cost functions that look for similar object sizes and nearest neighbors in the next frame. Iteration is then used to combine similar non-overlapping 3D trajectories [6].

A simple example of DIH for three-dimensional object localization is illustrated in Fig. 3. Here, a single laser beam is passed across a horizontal wire and measured with a camera focused on a plane that is a specified distance from the wire. The raw DIH image at $z = 97$ shows the wire with clear interference patterns. When numerically refocused to $z = 0$, the edges of the wire become sharper, indicating the z-location of the wire. Through this process, it is possible to locate multiple non-overlapping objects in three-dimensions using a single holographic image.

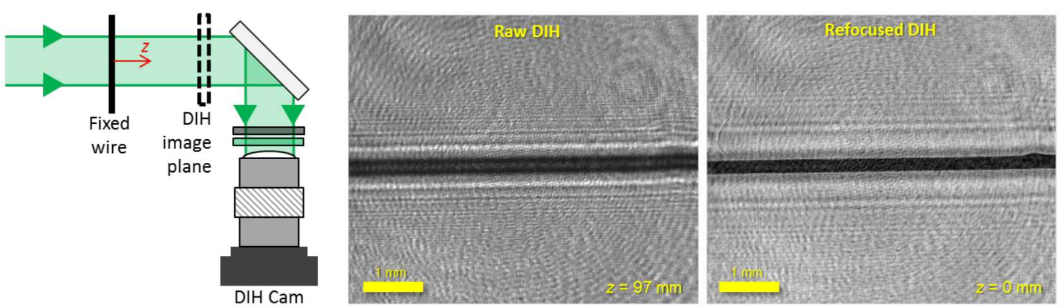

Figure 3: *Raw (at $z = 97$) and numerically refocused (at $z = 0$) digital in-line holograms of a fixed wire.*

3 SINGLE-SHOT MEASUREMENTS:

3.1 EXPERIMENTAL APPARATUS:

Phase conjugate digital in-line holography was first implemented using the degenerate four-wave-mixing topology shown in Fig. 4. This topology was chosen over spontaneous Brillouin scattering due to its compatibility with both picosecond and nanosecond laser excitation [33]. A low-repetition rate, regeneratively amplified picosecond laser (Ekspla PL2231C-20, 20 Hz, 80 ps, 532 nm, >15 mJ/pulse) is utilized to determine timing and alignment. Next, a modified Spectral Energies QuasiModo pulse-burst laser [15] is used to generate kHz to MHz rate laser light with pulse durations of 10 ns. The previous maximum operating rate of this laser was 1 MHz and was increased to 5 MHz with custom software upgrades. This pulse burst laser contains a pulsed seed source with 2 GHz bandwidth, two double pass diode-pumped amplifications stages, two double pass 9 mm diameter flashlamp-pumped amplification stages, and two single pass 12 mm diameter flashlamp-pumped amplification stages. The burst duration was set to 1.5 ms or lower to maximize flashlamp voltage and energy per pulse. The amplified 1064 nm is then passed through a telescope and doubled to 532 nm in a 10 mm diameter KTP crystal. The operation of the two lasers is alternated depending on the application via a flip mirror.

After exiting the lasers, the 532 nm light is first passed through a two-stage attenuator consisting of half-wave plates and thin film polarizers. The light then passes through a 15 mm diameter

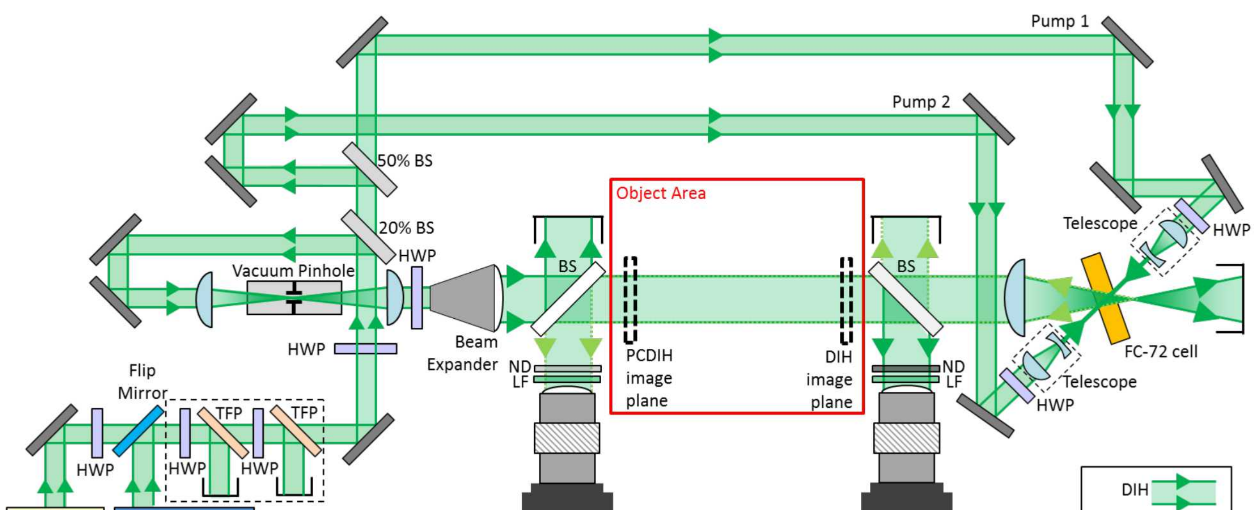

Figure 4: *Simplified experimental setup for phase conjugate digital in-line holography implemented using degenerate four-wave mixing for picosecond and nanosecond lasers. (HWP–half wave plate, TFP–thin-film polarizer, BS–beam splitter, ND–neutral density filter, LF–laserline filter 0.2 nm FWHM bandwidth)*

Electro-Optics Technology isolator and a vertical periscope (not shown in the figure). The light is then split into one imaging beam and two additional pump beams. The imaging beam passes through a delay stage, a vacuum pinhole spatial filter (300 mm FL lenses, 100 μm pinhole), and a beam expander (2$\times$ or 3$\times$) before reaching the PCDIH camera pick-off mirror (5% reflectivity) and entering the object area. After 5% of the light is directed into the DIH camera via another pick-off mirror, the remaining light is focused through a heavy fluorocarbon 3M FC-72 fluid cell (AR coated 1 mm thick windows, 10 mm thick cell).

Two counter-propagating pump beams are also passed through the cell such that all three beams intersect slightly before the focal point of the imaging beam (to prevent breakdown and damage to the windows). All three pulses are precisely timed via delay stages to arrive at the cell simultaneously. When using the pulse-burst laser, the pump beams utilize additional telescopes to control beam collimation and to increase the power density of beams within the cell. The angle of the pump beams with respect to the imaging beam is approximately 23°. Polarization of all three beams are also precisely controlled (p-, p-, and s-polarizations for the imaging, pump 1, and pump 2 beams respectively) to maximize the PCDIH signal (dotted green lines, s-polarization). The phase conjugate signal generated inside the cell back propagates along the imaging path, through the object area, and 5% of the light is finally directed into the PCDIH camera. The overlap of the two counter-propagating pump beams is critical to producing overlap of the incoming imaging beam and the phase conjugate return signal.

For low repetition rate imaging, LaVision sCMOS (2560 $\times$ 2160 pixels, 6.5 μm pixel pitch, 16-bit depth) cameras can be used to acquire data through Infinity K2 DistaMax long distance microscopes (with CF-2 or CF-3 lenses). For MHz-rate imaging, ultra-high-speed cameras are required. Here, we utilize Shimadzu HPV-X2 cameras capable of operating at 5 MHz rates in full frame mode (400 $\times$ 250 pixels, 32 μm pixel pitch, 10-bit depth). The cameras were triggered with the laser burst signal. Synchronization with respect to the each pulse in the burst was not required due to the low number of frames (128 frames max). Neutral density filters are added to adjust the intensity and laserline filters are added to minimize light generated by plasmas or explosive emissions.

3.2 SUPERSONIC STATIONARY SHOCK-WAVES:

A comparison of measurements taken with a normal mirror versus a phase conjugate mirror is shown in Fig 5. For this experiment, the focal plane of the PC camera and normal camera are placed at the image plane at the centerline of a supersonic stationary shock-wave generated by a Mach 3.4 air jet (6.35 mm nozzle outlet, stagnation pressure 5.5 MPa, atmospheric pressure 84 kPa). The images generated using the high beam-quality, low repetition-rate picosecond laser show frames taken from the normal camera, the phase-conjugate camera utilizing the lens and phase conjugate cell, and the phase-conjugate camera where the lens and cell are replaced with a 90° normal mirror.

With the normal camera, the shock-wave edges are sharp and clearly visible due to refraction

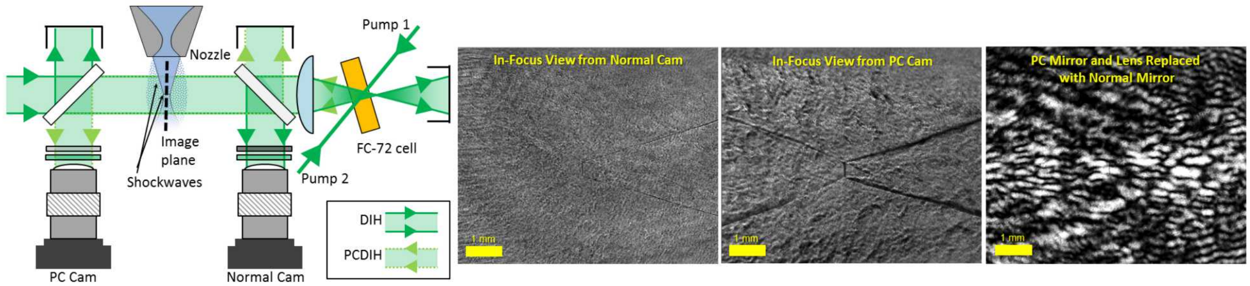

Figure 5: *An phase-conjugate and normal imaging setup is illustrated using a picosecond laser to obtain in-focus images of shock-waves in a Mach 3.4 supersonic jet. The left-most image shows the in-focus jet from the normal camera, the middle image shows the in-focus jet from the phase conjugate camera, and the right-most image show the in-focus jet when the phase conjugate cell and lens are removed and replaced with a 90° normal mirror.*

at the shock-wave edges. Small turbulent disturbances in the gases surrounding the shock are also visible. This can be compared with the phase-conjugate image. Since the illumination source is a coherent, interference patterns are generated by light that is scattered from the shock-wave edges. When these interference patterns and other phase distortions enter the phase-conjugate cell, the phases are reversed and travel back through the shock-wave, thereby correcting much of the distortion. However, in the phase-conjugate image, the shock-wave edges as well as the turbulent disturbances are more clearly visible. This is likely due to several effects. First, the phase-conjugate system double passes light through the same disturbance thereby increasing absorption. Second, depending on the design of the lenses, a degenerate four-wave-mixing phase-conjugate system is capable of rejecting light that is slightly refracted by the three-dimensional curvature of the shock-wave or disturbance, thereby enhancing shock-wave edges. This effect is explored further in Section 5.

These images can be compared with the image taken where the phase-conjugate camera where the lens and cell are replaced with a normal mirror. A normal mirror does not correct for phase disturbances or any of the interference patterns generated during the first pass. Therefore, the shock-wave disturbance from the first pass are distorted in this case to give very strong interference patterns. The set of shock-wave edges that are visible in this image are due purely to light refracted during the second pass through the shock-wave. These images clearly illustrate differences in the operation of normal versus phase-conjugate imaging in the presence of a phase disturbance.

Next, the focal planes of the two cameras are moved for holographic measurements as illustrated in Fig. 6. The focal planes for DIH and PCDIH were both placed $\sim$97 mm from the wire such that the magnification of the two systems match. The top row illustrates single-shot images refocused to the centerline of the shock-wave. The shock-wave edges are clearly visible in the PCDIH images while the DIH images are unable to refocus clearly to shock-wave edges. Comparing Fig. 5 and 6, it is clear that imaging degrades significantly when imaged out-of-focus and

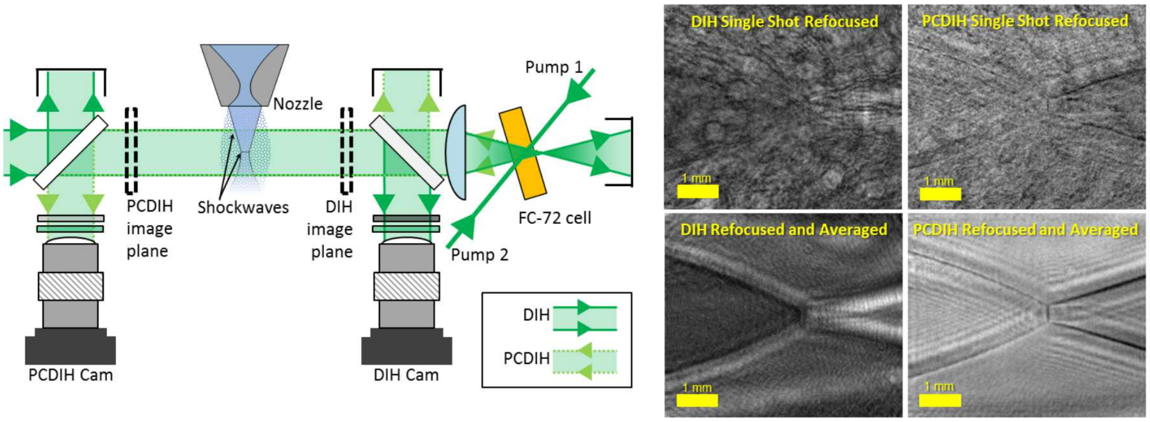

Figure 6: *A PCDIH and DIH imaging setup is illustrated using a picosecond laser to obtain holograms of shock-waves in a Mach 3.4 supersonic jet. The top row shows single-shot holograms refocused to the centerline of the shock-waves illustrating both the shocks and local turbulence distortions. The bottom row shows averaged (500 images) holograms refocused to the centerline of the shock-waves.*

then numerically refocused for DIH. For PCDIH, imaging quality degradation is also noticeable but shock-wave edges can still be recovered via numerical refocusing.

The bottom row of images removes the random turbulence effects in the images by averaging 500 different shots. While the averaged PCDIH refocused image shows all the shock-waves clearly, the traditional DIH is unable to refocus to any of the the shock-wave edges after averaging. The inability to refocus the traditional DIH images is most likely due to the dominance of the uncorrected time- and spatially-varying phase delays (imparted by the jet density gradients and turbulence) when compared to the interference patterns generated by refraction at shock-wave edges. In PCDIH, only the refraction losses (which can be treated like absorptive losses) at shock-wave edges are present and can thus be refocused. These examples illustrates some of the benefits of using a phase-conjugate configuration for imaging.

3.3 LASER-SPARK PLASMA-GENERATED SHOCK-WAVES:

In order to test distortion correction capabilities of PCDIH in the presence of absorptive objects, a 200 μm diameter fixed wire is imaged with DIH and PCDIH using the picosecond laser as illustrated in Fig. 7. The focal planes for DIH and PCDIH were both placed $\sim$61 mm from the wire such that the magnification of the two systems match. A focused nanosecond laser (Continuum Surelite III, 10 Hz, 1064 nm, 5 ns pulse duration, 400 mJ per pulse) is then used to generate a spark at a distance of 15 mm from the wire, producing shock-waves that distort the wire profile. Holograms are captured $\sim$400 ns after the arrival of the laser spark.

The top row of images in Fig. 7 shows a raw hologram of the wire, a raw traditional DIH image with the shock-wave, and a raw PCDIH image with the shock-wave. The bottom row of

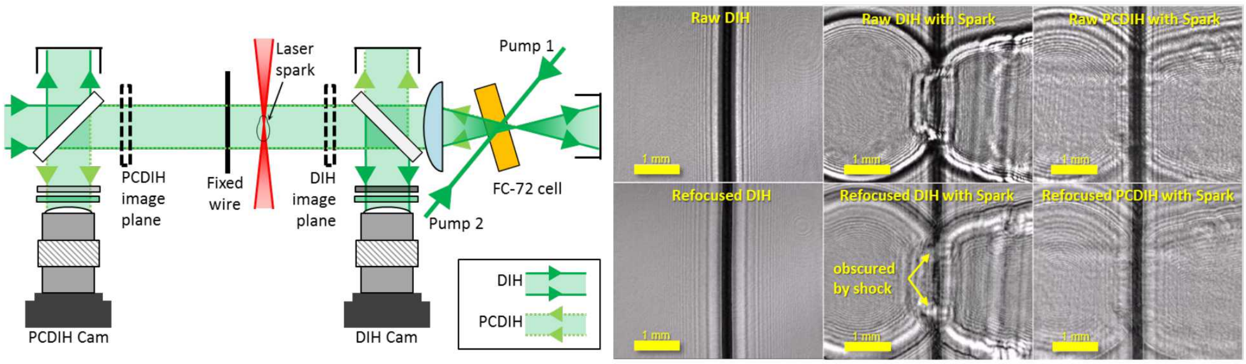

Figure 7: *Holograms of a fixed wire and shock-waves generated by a laser spark are illustrated. The top row shows the raw holograms of the wire, wire with a spark imagined using traditional DIH, and a simultaneous image of the wire with a spark imaged with PCDIH. The bottom row shows the same three holograms refocused to the focal plane of the wire. Images provided courtesy of [33].*

images shows the holograms refocused to the plane of the wire. With traditional DIH, the edges of the wire are completely distorted due to phase variations produced by density gradients which impose phase delays. With PCDIH, however, the edges of the wire are clearly visible and only slightly distorted by the shock-wave. On average (over 500 different laser-spark images) the wire edge in the DIH signal shows $\sim 8\times$ more distortion than the PCDIH signal [33]. When the laser spark is moved to the opposite side of the wire, the imaging beam interacts with the distortion before reaching the wire, so more distortion is expected from the perspective of the PCDIH camera. Measurements confirm that the wire edge distortion increases slightly for this second configuration for both holography systems (DIH distortion increases by 100%, PCDIH distortion increases by 46%) but the DIH signal still has $\sim 11.7\times$ more distortion than the PCDIH signal [33].

Two additional features can be noted from this experiment. First, the DIH image has slightly higher spatial resolution than the PCDIH image. The standard deviation of the wire edge with no spark is 0.6 μm for DIH and 1.9 μm for PCDIH [33]. One of the contributors to this effect is the amplitude shadow generated by the laser beam on its first pass over the wire. This shadow is designed to overlap the absorption from the second pass but can decrease edge contrast if any of the three beams (imaging, pump 1, or pump2) are not perfectly collimated.

Second, the DIH image appears to have more dynamic range than the corresponding PCDIH image with brighter shock-wave interference fringes. This effect is noted in all subsequent PCDIH results. The brighter interference pattern fringes in DIH are thought to be caused mostly by the phase delays and hence cannot be numerically refocused with traditional DIH algorithms. In PCDIH, the phase delay effects are canceled and only the refractive losses (which can be treated like absorptive losses) generated by shock-wave edges produce interference patterns that can be numerically refocused to the shock-wave edge. These images and quantitative results show that PCDIH can remove the phase-distortion produced by shock-waves on absorptive objects.

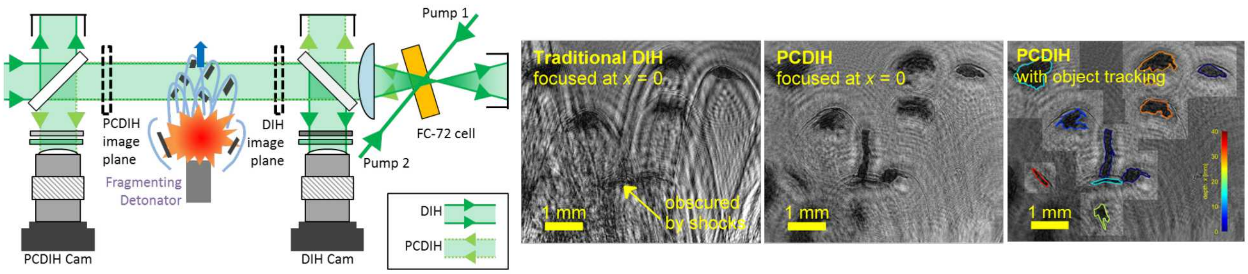

Figure 8: Holograms of a fragmenting detonator (pointing upward) using the picosecond laser are illustrated. Refocused images of objects obtained using the traditional DIH camera shows objects obscured by shock-wave distortions (left). However, the simultaneously obtained PCDIH frame (middle) eliminates much of the shock-wave distortion making the objects behind shock-waves visible. These objects are tracked with custom algorithms to show each fragment in their individual focal planes. Images provided courtesy of [33].

3.4 EXPLOSIVELY-GENERATED HYPERSONIC FRAGMENTS:

Next, the picosecond laser was applied to obtain single-shot images of a small fragmenting explosive detonator, as illustrated in Fig. 8. For these experiments [33], the optics are protected using a polycarbonate boom box that is placed inside the object area. The detonator ignites and fragments from aluminum foil covering the top of the detonator are launched into the imaging beam at 2 to 2.5 km/s [14]. These hypersonic fragments traveling at Mach 5.8 to 7.2 generate strong shock-waves surrounding the fragments. From the images, the leading fragments can be partially visualized with traditional DIH while fragments traveling slightly behind are distorted by the shock-waves of the leading fragments [14]. The refocused traditional DIH image in Fig. 8 shows this effect. The simultaneously obtained refocused PCDIH image, however, shows significantly less distortion. For example, one large fragment in the center of the image that was obscured in traditional DIH is easily visible in the PCDIH. This data illustrates how this technique can be used in explosive environments for 3D object tracking [33].

4 TIME-RESOLVED ULTRA-HIGH-SPEED MEASUREMENTS:

While interesting results can be obtained using a low repetition-rate, high beam-quality picosecond lasers, measurements with a pulse-burst nanosecond laser are required for operation at ultra-high-speeds in order to obtain videos of objects in transient explosive and supersonic environments. As illustrated in this work, systems like laser-spark plasma-generated shock-waves and explosives can vary significantly from test to test. Thus time-resolved measurements can provide additional information such as object or shock-wave speed for these transient events.

Sandia National Laboratories is a multimission laboratory managed and operated by National Technology and Engineering Solutions of Sandia, LLC, a wholly owned subsidiary of Honeywell International, Inc., for the U.S. Department of Energy's National Nuclear Security Administration under contract DE-NA-0003525.

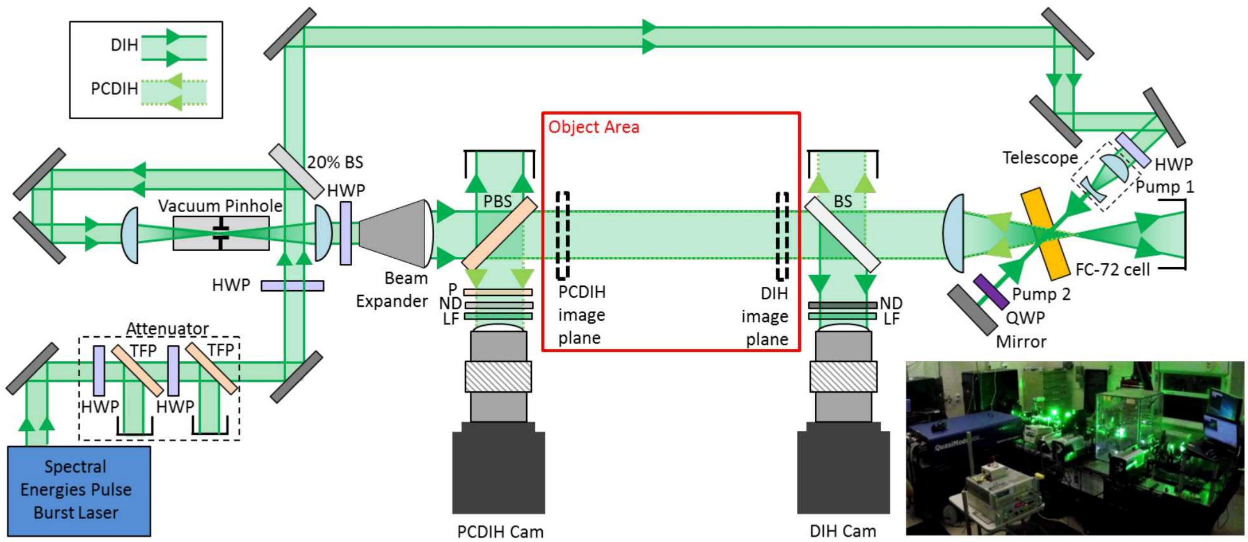

Figure 9: *Simplified experimental setup for phase conjugate digital in-line holography for the nanosecond pulse-burst laser. An image of the setup with the boombox during an explosive detonator experiment is shown in the inset. (HWP–half wave plate, QWP–quarter wave plate, TFP–thin-film polarizer, BS–beam splitter, PBS–polarizing beam splitter, P–polarizer, ND–neutral density filter, LF–laserline filter 0.2 nm FWHM bandwidth)*

4.1 EXPERIMENTAL APPARATUS FOR THE PULSE-BURST LASER:

For a nanosecond laser system with longer pulse durations and coherence lengths, a more efficient configuration similar to [34] can be utilized to produce more phase-conjugate signal, as illustrated in Fig. 9. Here, pump 1 is reflected from a 90° mirror and the polarization is rotated with a quarter wave plate to produce p-, p- and s-polarization at the imaging beam, pump 1 beam and pump 2 beams, respectively. By reusing the same beam for both pumps, more energy can be directed into the pumps, fewer components are needed, and alignment is simplified. Since bursts from the laser only occur once every 12 seconds, the overall alignment difficulty increases significantly when compared to the 10 Hz picosecond laser.

In order to collect more signal from the phase conjugate beam, the 5% beam splitter was replaced with a 45° polarizing beam splitter that reflects mostly s-polarized light directed toward to the PCDIH camera. Since the phase-conjugate signal is s-polarized in this design, this configuration also helps to reject background light and reduce p-polarized reflections from objects. Due to the high pulse and burst energies of the pulse-burst laser, additional care is taken expanding beams and shortening the burst duration to prevent damage to optics.

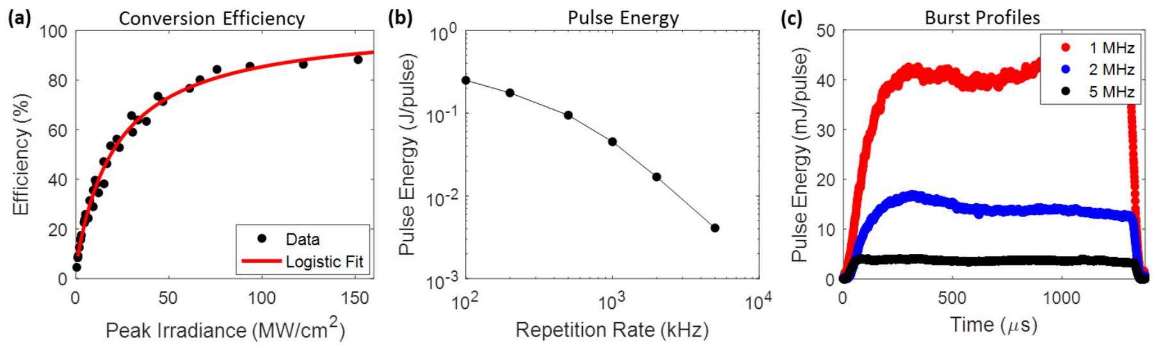

Figure 10: *(a) Second harmonic conversion efficiency, (b) energy per pulse at 532 nm, and (c) 532 nm burst profiles showing the peak energy of each pulse during the burst.*

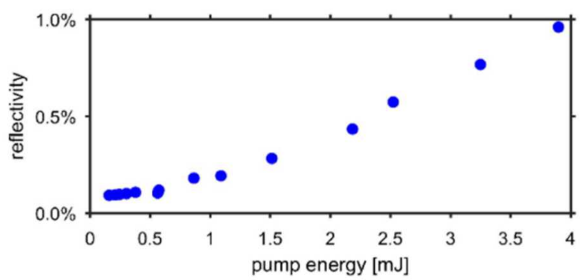

Figure 11: *Phase conjugate mirror efficiency is illustrated for the picosecond laser [33].*

4.2 SYSTEM CHARACTERIZATION:

While pulse-burst lasers have sufficient 532 nm pulse energy to generate phase conjugate signals at rates of tens or hundreds of kHz, the pulse energy drops significantly at MHz rates. This is due to two effects. First the increased repetition rate of the 1064 nm light depletes energy from the flash-lamp-pumped amplification media at a faster rate such that each pulse in the burst has a lower pulse energy. This lower pulse energy then decreases the nonlinear second harmonic conversion efficiency, further decreasing the pulse energy at 532 nm as illustrated in Fig. 10(a). The resulting maximum pulse energy at 532 nm and peak energy of each pulse in the burst are illustrated in Fig. 10(b) and (c). From these plots, it is clear the maximum pulse energy drops significantly as the repetition rate is increased.

Since four-wave mixing is a nonlinear process, the phase-conjugate signal conversion efficiency also tends to decrease as the pulse energies decrease. Figure 11 illustrates the decrease in reflectivity efficiency as a function of the pump energy in the imaging beam (with pump beam energies fixed). The drop in reflectivity is more pronounced when the energy of all three beams is decreased. Futhermore, the conversion efficiency of picosecond beams is better than nanosecond beams due to their relative peak intensities. These characteristics illustrate some of the challenges encountered when increasing the imaging repetition rates to ultra-fast regimes.

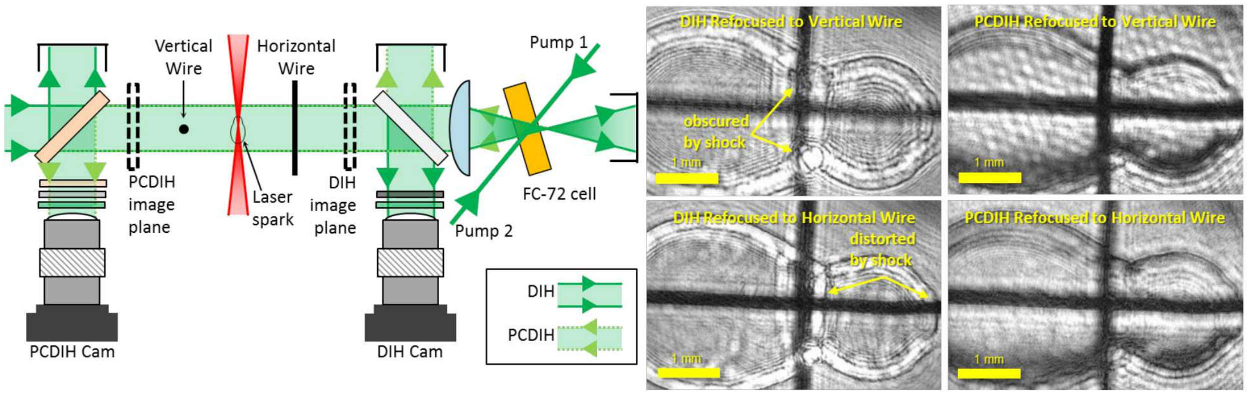

Figure 12: *Holograms of a laser-spark plasma-generated shock-wave using the pulse-burst nanosecond laser operating at 500 kHz are illustrated. A vertical wire and a separate horizontal wire are placed on either side of the laser spark. The top row of images shows holograms refocused to the vertical wire and the bottom row of images shows holograms focused to the horizontal wire. Traditional DIH images on the left show the vertical wire distorted by the shock-wave. PCDIH images on the right show no distortion of the refocused wires. Note that the overall image brightness was increased to improve visibility and that the pixels are not saturated.*

4.3 LASER-SPARK PLASMA-GENERATED SHOCK-WAVES:

The laser-spark plasma-generated experiment was repeated utilizing the nanosecond pulse-burst laser as illustrated in Fig. 12 for a repetition rate of 500 kHz. In this experiment, two crossed wires are used to illustrate some of the effects of the order of phase distortions and absorptive objects. A vertical wire is placed ∼12 mm to the left of the laser spark and a horizontal wire is placed ∼12 mm to the right of the laser spark. The imaging planes of the two cameras are then placed 20 to 40 mm from the laser spark. The top row illustrates the data refocused to the vertical wire while the bottom row illustrates the data refocused to the horizontal wire. The DIH images (left) show the strong shock-wave phase-distortions on the vertical wire and weak distortions on the horizontal wire. The corresponding DIH images show significantly reduced distortion to both wires at the cost of reduced spatial resolution due to the return shadow. The reduced dynamic range of the PCDIH images are noticeable when compared to the DIH, thus illustrating that the phase-conjugate system is properly correcting the bright interference patterns from phase-delays imparted by the shock-waves.

Several additional features can be noted from these images. First, the beam quality of the nanosecond pulse-burst laser is significantly poorer than the picosecond laser. Because the beam profile and intensity can change from burst-to-burst (and more slowly during the duration of the burst), obtaining background images for normalization is also more difficult. Overall, this results in poorer image quality and additional imaging artifacts. Since an ultra-high-speed camera with a low number of pixels is used, the resolution is also reduced when compared to the picosecond

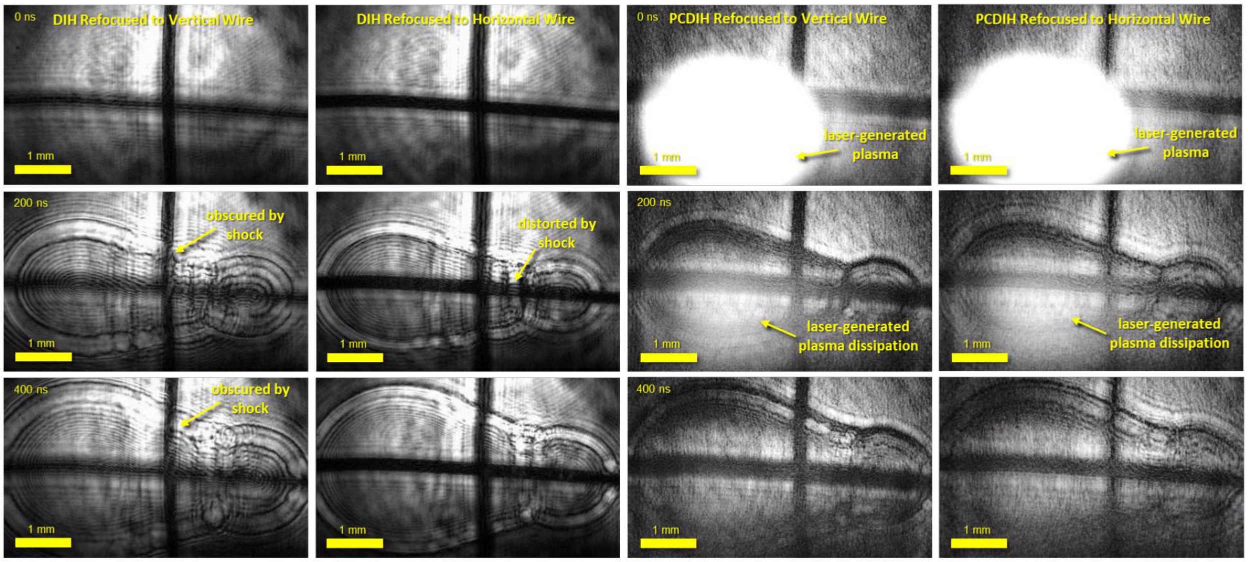

Figure 13: *Holograms of a laser-spark plasma-generated shock-wave using the pulse-burst nanosecond laser operating at 5 MHz are illustrated. The left two columns show traditional DIH images refocused to the vertical and horizontal wire and the right two columns show PCDIH images. The three rows show images taken at $t = 0$ ns, $t = 200$ ns, and $t = 400$ ns. Operating at 5 MHz, most of the ND filters must be removed thus making laser plasma emission visible in the PCDIH images.*

laser results. Second, a stronger return shadow is visible near the edges of the shock-wave in the PCDIH images. This effect is partially caused by the poorer divergence of the pulse-burst laser beam and partially caused by the the edge enhancement effect described in Section 5.

Operating at 500 kHz, it is only possible to catch a single frame of the laser-spark plasma-generated shock-wave edges inside the field-of-view. Thus, higher repetition rates are required to image these the transient events. As the repetition rate is increased to 1 MHz, 2 MHz, and 5 MHz, the phase conjugate mirror efficiency drops, the signal-to-noise ratio decreases, and the neutral density filters in front of the cameras need to be reduced in order to measure signal. One example of a simultaneous PCDIH and DIH at 5 MHz is illustrated in Fig. 13. The two columns on the left illustrate images taken with the DIH camera refocused to the vertical and horizontal wires. The two columns on the right illustrate images taken from the PCDIH camera. At 5 MHz, the reduction in neutral density filters for the PCDIH camera allows the plasma emission at 532 nm to overwhelm the phase conjugate signal at $t = 0$. As time progresses to $t = 200$ ns, the plasma emission begins to dissipate and by $t = 400$ ns, the shock-wave can be more clearly seen. Because significantly more DIH signal is available and more neutral density filters can be used, the plasma emission was not visible at $t = 0$ for DIH. However, when comparing $t = 200$ ns and $t = 400$ ns, distortions of the wire are visible on the DIH cameras and reduced on the PCDIH cameras.

A time series of the shock-wave expansion recorded via PCDIH is illustrated in Fig. 14. For

Built on
LDRD
Laboratory Directed Research
and Development

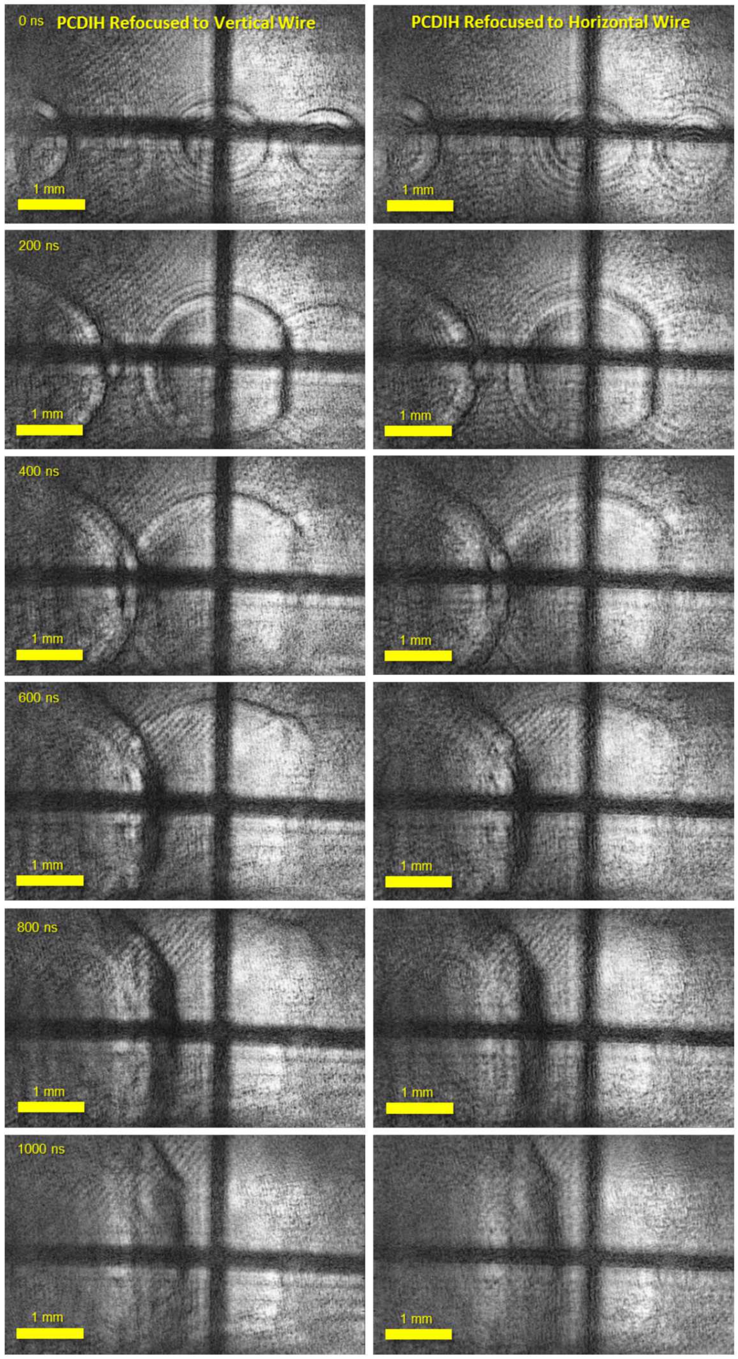

Figure 14: *Holograms of a laser-spark plasma-generated shock-wave using the pulse-burst nanosecond laser operating at 5 MHz are illustrated. For this weaker laser-spark, the plasma is less visible.*

Sandia National Laboratories is a multimission laboratory managed and operated by National Technology and Engineering Solutions of Sandia, LLC, a wholly owned subsidiary of Honeywell International, Inc., for the U.S. Department of Energy's National Nuclear Security Administration under contract DE-NA-0003525.

this particular case, the laser plasma is only slightly visible at the left edge of the images at $t = 0$. From these images, it is possible to track the growth rate of the shock-wave edge over time as well as visualize the interaction of multiple shock-waves as they meet.

4.4 EXPLOSIVELY-GENERATED HYPERSONIC FRAGMENTS:

Explosively-generated hypersonic fragments are measured using the ultra-high-speed PCDIH system, as illustrated in Fig. 15 at 2 MHz. In this experiment, the detonator (custom RP-80 with a 180 μm-thick brass cap) is pointed such that all the fragments travel downward. The left column shows measurements obtained using the DIH camera and the right column shows measurements obtained using PCDIH. Note that the overall image brightness was increased to improve visibility and that the pixels are not saturated. The first frame illustrates sub-millimeter particles ejected slightly ahead of a group of larger fragments. From the DIH images, the sub-millimeter fragments are clearly visible and numerically re-focusable. The first group of large particles in DIH, however, are partially obscured by the bright interference fringes from phase distortions. Subsequent particles that lag behind the first group are even more severely obscured. As illustrated earlier, the shock-wave edges and fragments near the interference patterns generated from phase distortions cannot be numerically refocused.

In the PCDIH images, however, the sub-millimeter particles, first group of large particles, as well as the subsequent particles are more clearly visible and can be readily refocused to determine their relative z-positions. With ultra-high-speed video, it is also possible to visualize particle motions including small particle rotations over time.

Experiments at 5 MHz were also conducted as part of this study, but showed significantly lower signal-to-noise and increased reflections (even with the use of polarizers) from the brass fragments generated by the detonator. This is mostly due to the drop in phase-conjugate signal and corresponding reduction of neutral density filtering. The double-pass configuration of PCDIH makes it more susceptible to reflections from the first pass of the laser light. In contrast, the backlit orientation of the DIH system with respect to the object and laser source makes it much less susceptible to reflections even with no neutral density filtering.

5 SHOCK-WAVE EDGE ENHANCEMENT:

One interesting feature of the four-wave-mixing phase-conjugate configuration utilized in this study is the enhancement of shock-wave edges via a shadow-like effect. This is most clearly illustrated in Fig. 16. This example shows the conventional DIH image of a shock-wave and the corresponding image with PCDIH where a 300 mm FL lens is used before the phase-conjugate cell. In the right-most image, however, a 125 mm FL lens is used instead and the shadow intensity is significantly reduced. This adjustable shock-wave edge enhancement effect is due to the four-wave-mixing configuration and is schematically illustrated in Fig. 17. As light passes through a density gradient, such as a semi-spherical plasma-generated shock-wave, light near the edges are

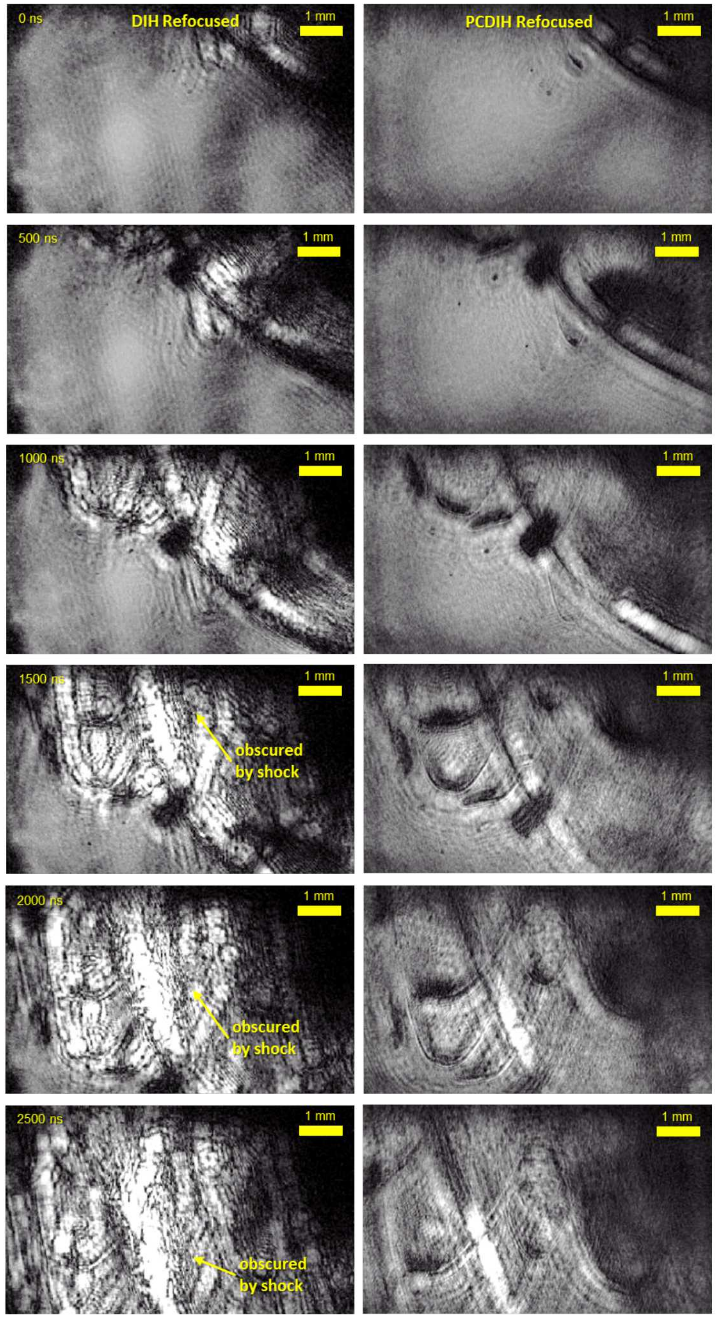

Figure 15: *Holograms of a fragmenting detonator (pointing downward) using the pulse-burst nanosecond laser are illustrated operating at 2 MHz. Late arriving fragments are obscured in traditional DIH images (left) by shock-wave interference patterns. However, they are visible in the PCDIH images (right).*

Sandia National Laboratories is a multimission laboratory managed and operated by National Technology and Engineering Solutions of Sandia, LLC, a wholly owned subsidiary of Honeywell International, Inc., for the U.S. Department of Energy's National Nuclear Security Administration under contract DE-NA-0003525.

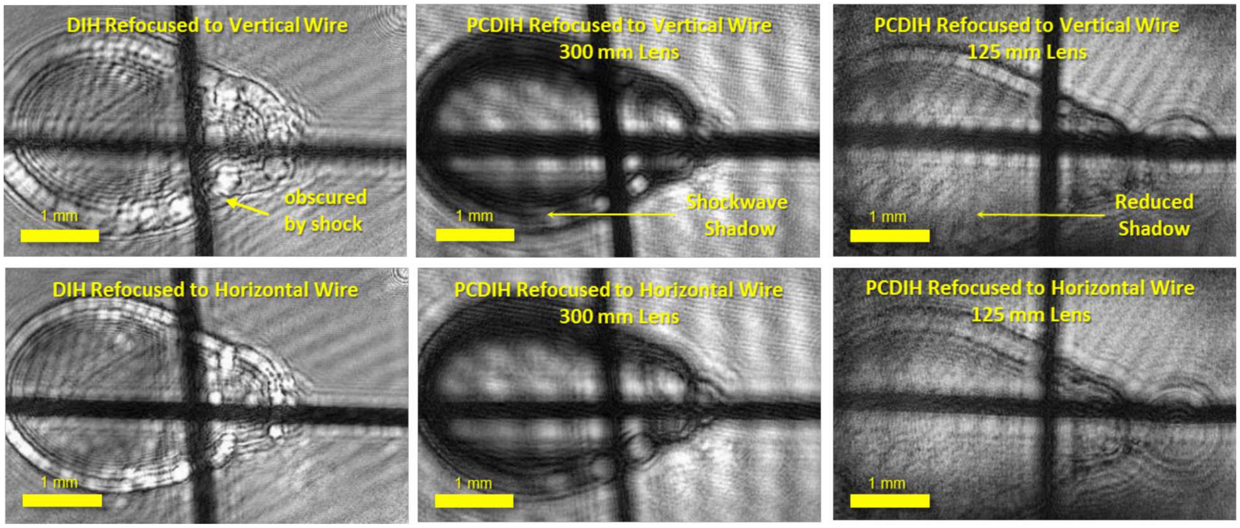

Figure 16: *Shock-wave edges can be enhanced using degenerate four-wave-mixing PCDIH. The left column shows traditional DIH images, the middle column shows PCDIH using a long focal-length lens (300 mm FL), and the right column shows PCDIH using a shorter focal-length lens (125 mm FL).*

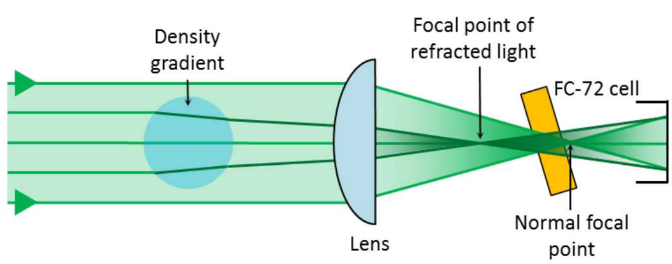

Figure 17: *A schematic demonstration of the preferential edge enhancement effect is illustrated. The light refracted by the density gradient focuses at a different position than the normal un-refracted light. The location of the two focal points with respect to the phase-conjugate cell determines the preferential enhancement effect.*

refracted at a small angle. When the refracted and un-refracted light reach the phase-conjugate cell, the un-refracted light is focused at one position and the slightly refracted light is focused at a slightly different position. This small difference in focal position is preferentially amplified by the phase conjugate cell (depending on where the focal points are located with respect to the cell) so that the normal, un-refracted light is brighter than the slightly refracted light.

If the focal length of the lens is longer, there is more separation between the focal points, thus enhancing the preferential reflection effects. Similarly, if the density gradient is stronger, the light is refracted at larger angles, also increasing this effect. Finally, the distance between the density gradient source and the lens can also alter the edge enhancement. This effect can be minimized or removed by using a shorter focal length lens.

This edge enhancement effect bears some similarity to schlieren techniques, due to its the ability to adjust the relative contrast from density gradients. However, schlieren measures the first derivative of the density gradient. This effect is also similar to shadowgraphy, which measures the second derivative of the density gradient. In this case, the preferential measurement of light refracted by the density gradient is aperture-free, non-linear, and conducted with coherent light. It has the additional benefit of canceling phase distortions and the ability to numerically refocus to the shock-wave edge and thus can be used for tracking multiple shock-wave edges in three-dimensions. Another potentially interesting feature is its ability to encode the refraction not as a phase delay but as an intensity level. With a model, some information could potentially be gathered on the three-dimensional shape of the shock-wave rather than simply the z-location of the refracted edge.

6 ANTICIPATED OUTCOMES AND IMPACTS:

Although we demonstrate that PCDIH successfully removes interference patterns from a variety of different types of density-driven phase-distortions, some remaining phase-distortion effects are still visible in the PCDIH images. The interference patterns measured at shock-wave edges are due mostly to refraction of the imaging beam because this effect is visible in both direct imaging and holograms of the shock-waves. However, the time-of-flight of light passing through the object, phase conjugate medium, and back through the object may also be sufficiently long ($\sim$2 ns) such that motion of the shock-wave is captured to produce additional distortions [33]. Some phase distortions near absorptive objects are also measurable in PCDIH images. This particular effect is due to the object and phase-delay order, but also due to the fact that phase-conjugation cannot correct for beam deflection effects [38]. More work is needed to understand, model, and minimize these remaining optical distortion sources. Additional follow-on research is necessary to help fully understand the accuracy, precision, and any possible fundamental limitations of this emerging diagnostic. In particular, it would be interesting to model the effects of density gradients, shock-wave curvature, and relative object location on the measurement of the remaining distortions noted in PCDIH using ray tracing techniques. A comparison of this model with experimental results would improve our understanding of the PCDIH process and would be valuable for determining if PCDIH would be effective for a given experimental arrangement.

To make this technology a production-level diagnostic, more work is needed to improve the instrument design to increase portability and overall system stability. Scaling the system for larger volume experiments is also of interest. Faster repetition rates, better beam-quality, and higher signal-to-noise ratios can potentially be achieved with existing technologies via additional upgrades to the pulse-burst laser and further system optimization. More laser energy or slower repetition rates can also lead to a tomographic capability using multiple PCDIH imaging beams. The upgrades conducted on the pulse-burst laser during this project will enable a variety of new ultra-high-speed diagnostic measurements. For example, megahertz spectroscopic methods for determining temperature, pressure, and chemical species concentrations are now possible. In addition, there are plans to use the higher-power ultra-high-speed repetition rate upgrades for the study of high frequency turbulence statistics using particle image velocimetry, for the generation of ultra-high-speed multi-pulse laser plasmas, and for ultra-fast time-resolved studies of soot generation.

One separate area of future study would be to explore the edge enhancement effect of the four-wave-mixing topology. More detailed modeling is needed to fully understand the parameters which control the effect as well as determine if shock-wave curvature can be estimated from measurements. New experiments would also be useful for determining the sensitivity of the enhancement effect. These measurements can be directly compared with schlieren and shadowgraphy to determine their relative sensitivities, especially in low pressure environments. This potentially has several high-altitude and hypersonic diagnostic applications.

Ultra-high-speed PCDIH has not been previously attempted. Thus, this work [39] has resulted in a significant technical leap-forward in three-dimensional diagnostics for extreme environments relevant to the NNSA and DoD mission spaces. Applications at Sandia include hypervelocity impact diagnostics, ejecta characterization, flyer plate characterization, and many other environments currently hindered by imaging through shock-waves. This diagnostic can be applied to existing explosives characterization projects for the Joint Munitions Program, Delivery Environments Program, and existing Laboratory Directed Research and Development (LDRD) projects focused on investigating small-scale explosives. Distortion canceling methods can also be applied to measure through hypersonic shock-waves, which is relevant to A4H LDRD and Strategic Partnership Programs.

The PCDIH edge-enhancement feature could also be used in the future as a high-sensitivity shock-wave edge detection method for low-pressure environments such as vacuum or inside Sandia's low-pressure Hypersonic Wind Tunnel. Our group is currently working with several facility owners who are interested in either eliminating shock-wave distortions or enhancing shock-wave edge sensing capabilities at low pressure. Based on our results, we hope to generate new LDRD proposals for further fundamental development of our techniques and to apply our new diagnostic capabilities to existing programs. This work has enabled temporally-resolved 3D measurements inside explosive environments without the need for experimental repetition or multiple views. Overall, this rapid six-month Exploratory Express LDRD effort has successfully demonstrated a proof-of-principle of the PCDIH technique at ultra-high-speeds in application-relevant R&D environments.

7 CONCLUSION:

This work implementing phase-conjugate digital in-line holography for three-dimensional imaging through shock-waves is the first to illustrate the technique at ultra-high-speeds up to 5 MHz.

Built on
LDRD
Laboratory Directed Research and Development

Previous demonstrations of this method were limited to 10 to 20 Hz due to the required laser energies [34, 33]. This work demonstrates up to five orders-of-magnitude increase in measurement speed thus enabling measurements of transient events such has laser-spark plasma-generated shocks, supersonic shock-waves, and explosively-generated hypersonic fragments.

PCDIH shows several advantages over traditional DIH. First, it reduces the interference patterns caused by phase distortions thus enabling numerical refocusing of shock-wave edges and removes distortions on absorptive objects such as high-speed fragments. This comes at the cost of slightly lower spatial resolution and increased measurement complexity. As the repetition rate of the laser is increased, the energy per pulse and the phase-conjugate mirror reflection efficiency decrease drastically, making ultra-high-speed measurements more challenging. At the highest repetition rates the PCDIH signal intensity can be lower than laser-plasma emissions or specular reflections from objects, thereby decreasing the signal-to-noise ratio. Damage to optical components can also occur. Despite these trade-offs, ultra-high-speed PCDIH shows particular promise for three-dimensional object tracking during transient events such as explosive detonations. Additionally, we show the capability to numerically refocus the shock-wave edges, which can be used to track the z-plane location of multiple shock-waves in explosively-generated hypersonic fragments. Finally, we also demonstrate a density-gradient edge-enhancement feature with this technique that can potentially be used in the future for high-sensitivity shock-wave detection.

ACKNOWLEDGMENTS:

We would like to thank Prof. Mikhail Slipchenko at Purdue University for providing software upgrades for operating the pulse burst laser at ultra-high-speeds. We would also like to thank Dr. Phillip L. Reu and Andres N. Baca (and the Explosives Technologies Group) for lending us Shimadzu ultra-high-speed cameras as well as Dr. Steven Beresh, Seth Spitzer, and Russell Spillers for lending us the pulse-burst laser. Marley Kunzler was invaluable for his assistance with setting up pressure systems.

REFERENCES:

[1] B. J. Jensen, K. J. Ramos, A. J. Iverson, J. Bernier, C. A. Carlson, J. D. Yeager, K. Fezzaa, and D. E. Hooks, "Dynamic experiment using IMPULSE at the Advanced Photon Source ," *J. Phys.: Conf. Ser.*, vol. 500, p. 042001, 2014.

[2] T. M. Willey, K. Champley, R. Hodgin, L. Lauderbach, M. Bagge-Hansen, C. May, N. Sanchez, B. J. Jensen, A. Iverson, and T. van Buuren, "X-ray imaging and 3D reconstruction of in-flight exploding foil initiator flyers," *J. Appl. Phys.*, vol. 119, p. 235901, 2016.

[3] Y. Chen, J. L. Wagner, P. A. Farias, E. P. DeMauro, and D. R. Guildenbecher, "Galinstan liquid metal breakup and droplet formation in a shock-induced cross-flow," *Int. J. Multiphase Flow*, vol. 106, pp. 147–163, 2018.

[4] Y. Chen, E. P. DeMauro, J. L. Wagner, M. Arienti, D. R. Guildenbecher, P. A. Farias, T. W. Grasser, P. D. Sanderson, S. W. Albert, A. M. Turpin, W. Sealy, and R. S. Ketchum, "Aerodynamic breakup and secondary drop formation for a liquid metal column in a shock-induced cross-flow," in *55th AIAA Aerospace Sciences Meeting, AIAA SciTech*, 2017. AIAA-2017-1892.

[5] D. R. Guildenbecher, J. L. Wagner, J. D. Olles, Y. Chen, E. P. DeMauro, P. A. Farias, T. W. Grasser, and P. E. Sojka, "kHz rate digital in-line holography applied to quantify secondary droplets from the aerodynamic breakup of a liquid column in a shock-tube," in *54th AIAA Aerospace Sciences Meeting, AIAA SciTech*, 2016. AIAA-2016-1044.

[6] D. R. Guildenbecher, M. A. Cooper, and P. E. Sojka, "High-speed (20 kHz) digital in-line holography for transient particle tracking and sizing in multiphase flows," *Appl. Opt.*, vol. 55, no. 11, pp. 2892–2903, 2016.

[7] Y. Chen, D. R. Guildenbecher, K. N. G. Hoffmeister, M. A. Cooper, H. L. Stauffacher, M. S. Oliver, and E. B. Washburn, "Study of aluminum particle combustion in solid propellant plumes using digital in-line holography and imaging pyrometry," *Combust. Flame*, vol. 182C, pp. 225–237, 2017.

[8] Y. Chen, D. R. Guildenbecher, K. N. G. Hoffmeister, and P. E. Sojka, "Digital imaging holography and pyrometry of aluminum drop combustion in solid propellant plumes," in *Proceedings of the Imaging and Applied Optics Conference: Laser Applications to Chemical, Security and Environmental Analysis*, 2016. LT4F.2.

[9] Y. Chen, J. D. Heyborne, and D. R. Guildenbecher, "Time-resolved digital in-line holography and pyrometry for aluminized solid rocket propellants," in *Proceedings of the Imaging and Applied Optics Conference: Laser Applications to Chemical, Security and Environmental Analysis*, 2018. LTu3C.5.

[10] D. R. Guildenbecher, M. A. Cooper, W. Gill, H. L. Stauffacher, M. S. Oliver, and T. W. Grasser, "Quantitative, three-dimensional imaging of aluminum drop combustion in solid propellant plumes via digital in-line holography," *Opt. Lett.*, vol. 39, no. 17, pp. 5126–5129, 2014.

[11] M. S. Powell, I. W. Gunduz, W. Shang, J. Chen, S. F. Son, Y. Chen, and D. R. Guildenbecher, "Agglomerate sizing in aluminized propellants using digital inline holography and traditional diagnostics," *J. Propul. Power*, 2018. [in press].

[12] D. R. Guildenbecher, J. Gao, P. L. Reu, and J. Chen, "Digital holography simulations and experiments to quantify the accuracy of 3D particle location and 2D sizing using a proposed hybrid method," *Appl. Opt.*, vol. 52, no. 16, pp. 3790–3801, 2013.

[13] D. R. Guildenbecher, P. L. Reu, H. L. Stauffacher, and T. W. Grasser, "Accurate measurement of out-of-plane particle displacement from the cross correlation of sequential digital in-line holograms," *Opt. Lett.*, vol. 38, no. 20, pp. 4015–4018, 2013.

[14] J. D. Yeager, P. R. Bowden, D. R. Guildenbecher, and J. D. Olles, "Characterization of hypervelocity metal fragments for explosive initiation," *J. Appl. Phys.*, vol. 122, no. 3, p. 035901, 2017.

[15] S. Beresh, S. Kearney, J. Wagner, D. Guildenbecher, J. Henfling, R. Spillers, B. Pruett, N. Jiang, M. Slipchenko, J. Mance, and S. Roy, "Pulse-burst PIV in a high-speed wind tunnel," *Meas. Sci. Technol.*, vol. 26, no. 9, pp. 095305–1 – 095305–13, 2015.

[16] J. B. Michael, P. Venkateswaran, C. R. Shaddix, and T. R. Meyer, "Effects of repetitive pulsing on multi-kHz planar laser-induced incandescence imaging in laminar and turbulent flames," *Appl. Opt.*, vol. 54, no. 11, pp. 3331–3344, 2015.

Built on
LDRD
Laboratory Directed Research and Development

[17] T. R. Meyer, B. R. Halls, N. Jiang, M. N. Slipchenko, S. Roy, and J. R. Gord, "High-speed, three-dimensional tomographic laser-induced incandescence imaging of soot volume fraction in turbulent flames," *Opt. Express*, vol. 24, no. 26, pp. 29547–29555, 2016.

[18] S. Roy, P. S. Hsu, N. Jiang, M. N. Slipchenko, and J. R. Gord, "100-kHz-rate gas-phase thermometry using 100-ps pulses from a burst-mode laser," *Opt. Lett.*, vol. 40, no. 21, pp. 5125–5128, 2015.

[19] F. Fuest, M. J. Papageorge, W. R. Lempert, and J. A. Sutton, "Ultrahigh laser pulse energy and power generation at 10kHz," *Opt. Lett.*, vol. 37, no. 15, pp. 3231–3233, 2012.

[20] M. E. Smyser, K. A. Rahman, M. N. Slipchenko, S. Roy, and T. R. Meyer, "Compact burst-mode Nd:YAG laser for kHz-MHz bandwidth velocity and species measurements," *Opt. Lett.*, vol. 43, no. 4, pp. 735–738, 2018.

[21] S. Sugawa, R. Kuroda, T. Takeda, F. Shao, K. Miyauchi, and Y. Tochigi, "A 20Mfps global shutter CMOS image sensor with improved sensitivity and power consumption," in *International Image Sensor Workshop*, pp. 166–169, 2015.

[22] G. S. He, "Optical phase conjugation: principles, techniques and applications," *Prog. Quant. Electron.*, vol. 26, pp. 131–191, 2002.

[23] D. P. Marrinan, F. Fuest, and J. A. Sutton, "Spatial resolution-preserving retroreflection for gas-phase laser scattering measurements in turbulent flames using a phase-conjugate mirror," *Opt. Lett.*, vol. 41, no. 3, pp. 468–471, 2016.

[24] D. M. Bloom and G. C. Bjorklund, "Conjugate wave-front generation and image reconstruction by four-wave mixing," *Appl. Phys. Lett.*, vol. 31, no. 9, pp. 592–594, 1977.

[25] J. M. Yarrison-Rice, E. J. Sharp, G. L. Wood, G. J. Salamo, R. Klank, and R. R. Neurgaonkar, "High-resolution phase-conjugate imaging in double-pumped phase conjugators," *Appl. Opt.*, vol. 34, no. 32, pp. 7597–7603, 1995.

[26] F. Devaux, G. le Tolguenec, and E. Lantz, "Phase conjugate imaging by type II parametric amplification," *Opt. Commun.*, vol. 147, pp. 309–312, 1998.

[27] B. Thurow, N. Jiang, M. Samimy, and W. Lempert, "Narrow-linewidth megahertz-rate pulse-burst laser for high-speed flow diagnostics," *Appl. Opt.*, vol. 43, no. 26, pp. 5064–5073, 2004.

[28] B. Fischer and S. Sternklar, "Image transmission and interferometry with multimode fibers using self-pumped phase conjugation," *Appl. Phys. Lett.*, vol. 46, no. 2, pp. 113–114, 1985.

[29] H. Kogelnik, "Imaging of optical modes–resonators with internal lenses," *Bell Syst. Tech. J.*, vol. 44, no. 3, pp. 455–494, 1965.

[30] A. O. A. Shibukawa, Y. Goto, S. Honma, and A. Tomita, "Digital phase conjugate mirror by parallel arrangement of two phase-only spatial light modulators," *Opt. Express*, vol. 22, no. 10, pp. 11918–11929, 2014.

[31] T. R. Hillman, T. Yamauchi, W. Choi, R. R. Dasari, M. S. Feld, Y. Park, and Z. Yaqoob, "Digital optical phase conjugation for delivering two-dimensional images through turbid media," *Sci. Rep..*, vol. 3, 2013.

[32] S. Toda, Y. Kato, N. Kudo, and K. Shimizu, "Effects of digital phase-conjugate light intensity on time-reversal imaging through animal tissue," *Biomed. Opt. Express*, vol. 9, no. 4, 2018.

[33] D. R. Guildenbecher, K. N. G. Hoffmeister, W. M. Kunzler, D. R. Richardson, and S. P. Kearney, "Phase conjugate digital inline holography (pcdih)," *Opt. Lett.*, vol. 43, no. 4, pp. 803–806, 2018.

Sandia National Laboratories is a multimission laboratory managed and operated by National Technology and Engineering Solutions of Sandia, LLC, a wholly owned subsidiary of Honeywell International, Inc., for the U.S. Department of Energy's National Nuclear Security Administration under contract DE-NA-0003525.

Sandia National Laboratories

U.S. DEPARTMENT OF ENERGY

[34] K. N. G. Hoffmeister, S. P. Kearney, and D. R. Guildenbecher, "Optical phase conjugate digital in-line holography for correcting aberations in particle-laden flames," in *54th AIAA Aerospace Sciences Meeting, AIAA SciTech*, 2016. AIAA-2016-1046.

[35] R. W. Hellwarth, "Generation of time-reversed wave fronts by nonlinear refraction," *J. Opt. Soc. Am.*, vol. A67, no. 1, pp. 1–3, 1977.

[36] J. Gao, D. R. Guildenbecher, P. L. Reu, and J. Chen, "Uncertainty characterization of particle depth measurement using digital in-line holography and the hybrid method," *Opt. Express*, vol. 21, no. 22, pp. 26432–26449, 2013.

[37] J. Gao, D. R. Guildenbecher, L. Engvall, P. L. Reu, and J. Chen, "Refinement of particle detection by the hybrid method in digital in-line holography," *Appl. Opt.*, vol. 53, no. 27, pp. G130–G138, 2014.

[38] K. N. G. Hoffmeister, D. R. Guildenbecher, and S. P. Kearney, "Hybrid fs/ps CARS for sooting and particle-laden flames," in *54th AIAA Aerospace Sciences Meeting, AIAA SciTech*, 2016. AIAA-2016-0282.

[39] Y. Chen, J. D. Heyborne, D. R. Guildenbecher, M. E. Smyser, and M. N. Slipchenko, "Ultra-high-speed pulse-burst phase conjugate digital in-line holography for imaging through shock-wave distortions," in *57th AIAA Aerospace Sciences Meeting, AIAA SciTech*, 2019.

Sandia National Laboratories is a multimission laboratory managed and operated by National Technology and Engineering Solutions of Sandia, LLC, a wholly owned subsidiary of Honeywell International, Inc., for the U.S. Department of Energy's National Nuclear Security Administration under contract DE-NA-0003525.